AIAA JOURNAL
Vol. 45, No. 1, January 2007

Technical Notes

TECHNICAL NOTES are short manuscripts describing new developments or important results of a preliminary nature. These Notes should not exceed 2500 words (where a figure or table counts as 200 words). Following informal review by the Editors, they may be published within a few months of the date of receipt. Style requirements are the same as for regular contributions (see inside back cover).

Boundary Layer on a Moving Wall

Eric Menu* and Stavros Tavoularis†
University of Ottawa, Ottawa, Ontario K1N 6N5, Canada

DOI: 10.2514/1.25752

Introduction

MOVING belts and other types of moving walls have been used as partial boundaries of wind tunnels, water channels, wings, and other facilities and components in many experimental investigations of a variety of flow phenomena. In applied studies, moving walls have been used to simulate the ground effect on moving vehicles [1–3] or as a means of boundary layer control and drag reduction [4–7], whereas moving belts have also been employed in fundamental investigations of the turbulence structure and associated heat transfer [8–13]. For a smooth, plane belt that is long enough to approximate the ideal case of an infinite moving wall and a uniform freestream, one would expect that the characteristics of the boundary layer (BL) would depend only on the relative velocity between the belt and the freestream. In practice, however, the operations of the belt and the flow facility could be coupled in apparent or subtle ways, and other factors may play a role in the near-wall velocity variation. Because it is not always feasible or economical to document directly the BL state under the actual experimental conditions, one may be compelled to adopt the use of information collected in conventional BL over stationary walls, even in moving-wall cases. This Note reports some experience in using a moving belt as the upper wall of a water channel, in the hope that it will be of help to other researchers using similar arrangements or planning to do so.

Experimental Facility and Procedures

The experiments were conducted in a closed-loop water channel with a free surface, having a test section that was 0.54 m wide, about 4.0 m long, and 0.75 m high, but filled with flowing water to a depth of 0.455 m, as shown schematically in Fig. 1. Part of the test section was covered by a continuous, smooth polyurethane belt, immersed by about 10 mm below the free surface. Particular effort was made to keep the belt taut and, as much as possible, planar on the side facing the flow, to avoid belt oscillations and curvature effects on the boundary layer. This was accomplished by means of three rollers, one of which was adjustable and also served as the drive, a backplate, and side clips, which reduced bowing. A number of other devices assisted in ensuring that its operation was as close to the ideal as possible. The belt could be moved forward or reversely at a constant speed U_w, which was measured by timing the passage of marks on it, within an uncertainty of 1%.

The local velocity of the water was measured with a laser Doppler velocimeter (Dantec) operating in single component, backscatter mode and with frequency shifting to allow reverse flow measurement. A transmitting–collecting lens with a focal length of 310 mm was used through a beam expander with a ratio of 1.95, resulting in a measuring volume that was 0.650 mm long and 0.078 mm in maximum diameter. The plane of the intersecting beams was oriented as to be parallel to the plane of the moving wall, so that measurements could be taken as closely as possible to it. The water was seeded with silicon carbide spheres, 1.5 μm in diameter, and the velocity statistics were transit time weighted to reduce velocity bias. Velocity measurements closer than about 0.2 mm to the wall were discarded, as they were found to be contaminated by wall effects. The Doppler signal was analyzed by a 16 bit burst processor (Dantec BSA F50), resulting in a velocity resolution of 0.015 mm/s. The streamwise x and transverse y axes are shown in Fig. 1. A brass rod, 4.8 mm in diameter was positioned in contact with the belt at $x = 30$ mm, to serve as a boundary layer trip.

The wall shear stress was estimated from the slope of the corresponding mean relative velocity profile very close to the wall, as [14]

$$\tau_w = \left[\mu \frac{\partial |U - U_w|}{\partial y}\right]_{y \to 0} \tag{1}$$

where U is the local mean (i.e., time averaged) flow velocity and μ is the viscosity of water. In all cases, significant linear regions were present, in conformity with the presence of a conventional viscous sublayer. The intersection of the linear fit to the viscous sublayer data with the horizontal axis was within 0.1 mm from the wall location that was determined by visual means. When reporting distances from the wall, it is the former location that was taken as the origin. Unlike high Reynolds number boundary layer studies, in which the viscous sublayer thickness is too small to permit the accurate measurements that are required for the application of Eq. (1), in the present case this method was deemed to be reliable, because the measuring volume of the laser Doppler velocimetry system was much smaller than the (relatively large) viscous sublayer thickness.

Although it was not possible to measure wall pressure either on the belt or any of the other water channel walls, which were made of solid glass, the streamwise pressure gradient, estimated roughly from measurements of the freestream velocity gradient, would be sufficiently small not to have an effect on the boundary layer development. In all cases, the freestream velocity depended mainly on the free surface slope on either side of the belt and the immersion depth of the belt. Boundary layer development along the test section would result in a slightly favorable pressure gradient, whereas the overall pressure field, within the boundary layer approximation, should not be affected measurably by wall motion.

Results

Measurements reported here were taken along the vertical centerplane of the water channel, at a streamwise location that was at about $x = 1600$ mm. Experiments were performed for three different combinations of the freestream velocity U_e and the wall velocity, all with the same freestream relative velocity

Received 8 June 2006; revision received 18 October 2006; accepted for publication 25 October 2006.

*Research Assistant, Department of Mechanical Engineering; Current Address: Climatair, 22 rue de la Dique, Nancy, France 54000.
†Professor, Department of Mechanical Engineering.

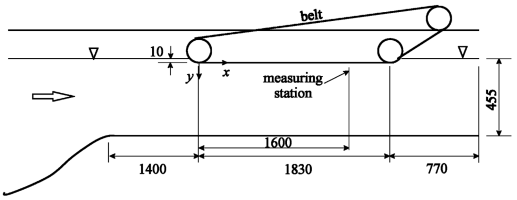

Fig. 1 Sketch of the flow facility; all dimensions in mm (not to scale).

$U_{r\max} = |U_e - U_w| = 0.34$ m/s. In the first case (to be denoted by WS) the wall was kept stationary, in the second case (WR) the wall was set in motion in a direction opposite to that of the freestream, and in the third case (WF) the wall was set in motion in the direction of the freestream but faster than it. A summary of all measured or calculated parameters is given in Table 1.

The local mean relative velocity of the flow was defined as $U_r = |U - U_w|$, where U is the local mean (i.e., time averaged) flow velocity; δ is the physical BL thickness (i.e., the distance from the wall at which $U_r = 0.99U_{r\max}$); δ^* is the displacement thickness; θ is the momentum thickness; $H = \delta^*/\theta$ is the shape factor; $Re_\theta = U_{r\max}\theta/\nu$ is the Reynolds number based on the momentum thickness (ν is the kinematic viscosity of water, in the present case equal to 9.2×10^{-7} m^2/s); $u^* = \sqrt{\tau_w/\rho}$ is the friction velocity; n is the exponent coefficient in the fitted power law

$$\frac{U_r}{U_{r\max}} = \left(\frac{y}{\delta}\right)^{1/n} \tag{2}$$

and B is the empirical constant in the logarithmic law

$$u^+ = \frac{1}{\kappa}\ell_n\, y^+ + B \tag{3}$$

in which $u^+ = U_r/u^*$, $y^+ = yu^*/\nu$, and κ is the von Kármán constant, taken as equal to 0.392. With respect to all thicknesses and Re_θ, the WS case is intermediate between the other two, with the WR case having the thickest BL and the highest Reynolds number. These parameters, however, depend on the streamwise location and cannot alone be used for comparisons, particularly because the definition of an effective BL origin becomes quite unclear when the wall is in motion. On the other hand, the shape factors H and the ratios δ/θ have comparable values for the three cases, thus indicating some macroscopic similarity in the three normalized relative velocity profiles. In closer examination, however (Fig. 2), these profiles display measurable differences. Whereas the WS profile can be fitted over its entirety by a power law with $n = 6.5$, in excellent agreement with values in the literature, both of the WR and WF profiles display deficits with respect to the WS case. This difference cannot be attributed to Reynolds number effects, because, if this were the case, the WR profile should have been in excess of the WS one, as being at a higher Reynolds number.

Plotted in logarithmic coordinates (Fig. 3), all three profiles have regions that can be fitted by power laws. Nevertheless, the extent of the power law region for the WS case ($0.04 \le y/\delta \le 1.0$) is much

Table 1 Summary of measured and calculated parameters

Parameter	WS	WR	WF	Units
U_e	0.34	0.18	0.10	m/s
U_w	0.00	−0.16	0.44	m/s
$U_{r\max}$	0.34	0.34	0.34	m/s
δ	51.8	78.8	35.3	mm
δ^*	7.0	11.8	5.5	mm
θ	5.3	8.8	4.0	mm
H	1.34	1.34	1.38	——
δ/θ	9.9	9.0	8.9	——
Re_θ	1950	3250	1470	——
n	6.5	5.4	4.9	——
u^*	13.9	12.9	13.4	mm/s
B	6.1	7.4	7.3	——

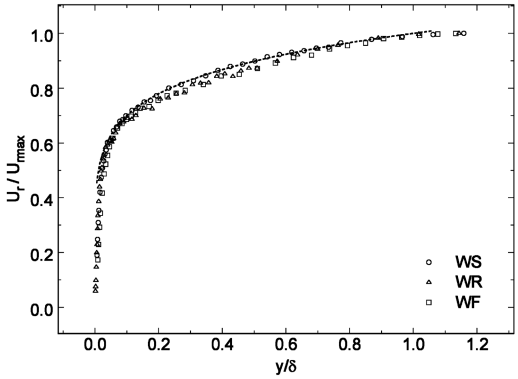

Fig. 2 Mean velocity measurements across the boundary layer; the dashed line is a power law, Eq. (2), fitted to the stationary-wall results.

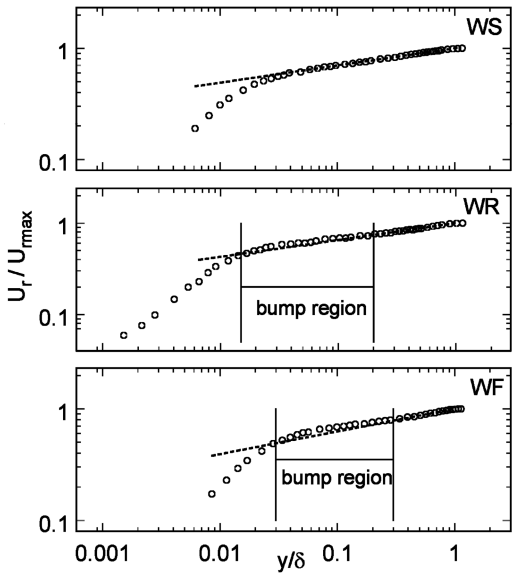

Fig. 3 Mean velocity measurements across the boundary layer in logarithmic coordinates; the dashed lines are power laws, Eq. (2), fitted to the outermost measurements.

wider than those for the WR ($0.2 \le y/\delta \le 1.0$) and WF ($0.3 \le y/\delta \le 1.0$) cases. Moreover, the values of the exponent n were 5.4 for the WR case and 4.9 for the WF case, both significantly smaller than that for the WS case. Observation of the measurements reveals that the local relative velocities were higher than values conforming to the corresponding power laws in the ranges $0.015 \le y/\delta \le 0.2$ for the WR case and $0.03 \le y/\delta \le 0.3$ for the WF case. In summary, wall motion appears to reduce the coefficient n in the power law, Eq. (2), restricting the range of the power law validity to the outermost BL and generating an excess of relative velocity in an intermediate range of distances from the wall. For descriptive purposes, we may call this intermediate range the "bump" in the relative velocity profile.

The previous scaling was based on the outer scales $U_{r\max}$ and δ. Let us now consider the three BLs in terms of the inner scales u^* and ν/u^* (viscous length). Figure 4 shows the mean relative velocity profiles for the three cases following inner scaling. Significant linear regions were present in all cases, in conformity with the presence of a viscous sublayer in which the velocity profile follows with the law

$$u^+ = y^+ \tag{4}$$

The values of the friction velocity were quite close to each other for the three cases, indicating that the innermost BL regions were comparable to each other. All three profiles can be fitted well by logarithmic laws, Eq. (2), with the same slope, but different values of the constant B. In the WS case, $B = 6.1$, very close to values in the

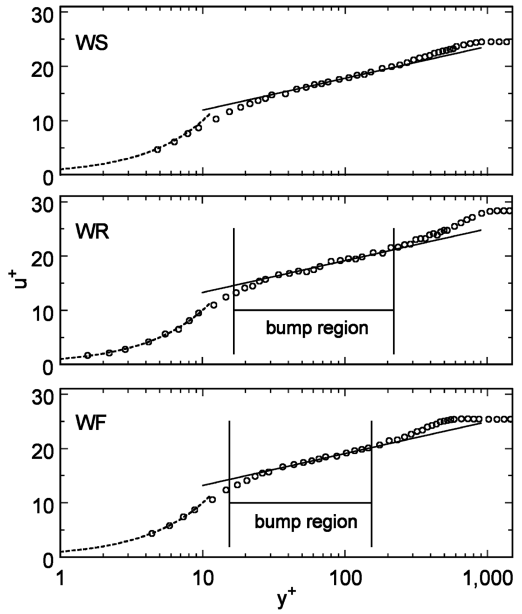

Fig. 4 Mean velocity measurements across the boundary layer in semilogarithmic coordinates; the dashed lines are the linear law, Eq. (4); the inclined solid lines are logarithmic laws, Eq. (3), fitted to the measurements.

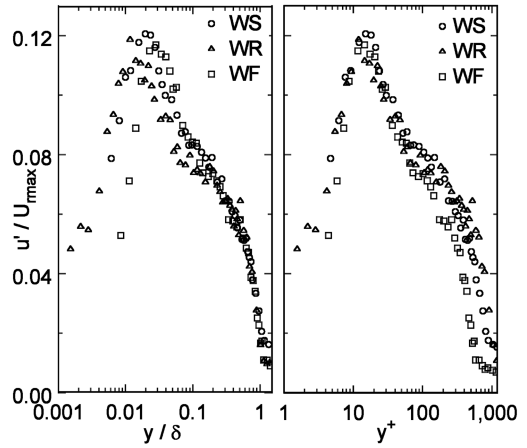

Fig. 5 Measurements of the normalized rms streamwise velocity fluctuation plotted vs distance from the wall normalized by the corresponding outer (left) and inner (right) length scales.

literature, whereas in the WR and WF cases, B took the measurably higher values 7.4 and 7.3, respectively, once more demonstrating excess in local relative velocity by comparison to stationary-wall BL results. The upper boundary of the logarithmic region in both moving-wall cases approximately coincides with the upper boundary of the bump region in the power law. Another interesting observation based on Fig. 4 is that wall motion in either direction increased the amplitude of the "wake function" in the outer BL above the stationary-wall value.

Finally, some evidence for the effect of wall motion on the BL turbulence is demonstrated by the variation of the rms streamwise velocity u', plotted in Fig. 5 vs inner- and outer-scaled distances from the wall. When plotted vs y/δ, the measurements of u' for the three cases collapse in the outer region beyond the bump but deviate elsewhere. When plotted vs y^+, the same measurements collapse in the inner region between the bump and the wall but deviate in the remainder of the BL. The variations of turbulence fluctuations with y^+ for the three cases are consistent with the relative locations of the wake function peaks, inferred from Fig. 4. In summary, the turbulence variation is scalable by appropriate laws outside the bump region but there is no scaling that will describe it within the bump region.

Discussion and Conclusions

As demonstrated in the previous section, wall motion, both reverse or forward, distorts the mean velocity profile and the turbulence in some intermediate range within the BL, while allowing conventional scaling in the viscous sublayer and an outermost sublayer. This intermediate range is characterized by a bump, namely, an excess of local relative velocity with respect to conventional profiles. In the case of reverse wall motion, the bump represents an absolute velocity surplus, whereas, in the case of forward wall motion, it represents an absolute velocity deficit. A plausible explanation for this discrepancy can be based on simple continuity considerations. At locations sufficiently upstream and downstream of the belt, one may assume that the velocity in the water channel is unaffected by belt motion and so is the mass flow rate across the test section. Under the belt, however, the situation changes. In reverse motion, the belt is continuously transporting fluid in its proximity from its downstream end to its upstream end. This fluid recirculates and moves forward within some region aligned with the belt but at some distance from it, thus generating the bump in relative velocity. Further away from the belt, this effect becomes negligible, permitting conventional scaling based on the velocity difference between the wall and the freestream. To test this hypothesis, we integrated the part of the absolute velocity profile that corresponded to negative velocities and found the flow rate in this region to be fairly close to the excess in flow rate represented by the bump. In forward motion, the belt transports an excess of fluid from its upstream end to its downstream end. Conforming with continuity, an absolute velocity deficit is generated at some intermediate distances from the wall, while further away this effect becomes negligible. Note that no amount of water was allowed to be transported around the entire belt, as both its ends were wiped continuously by foam pads.

In conclusion, the present results have demonstrated that the motion of a belt covering partially the free surface of a water channel distorts its boundary layer, both in mean velocity profile and turbulence distribution. Conventional boundary layer analysis based on relative velocity with respect to the wall will lead to discrepancies in a substantial region located between the viscous sublayer and an outermost sublayer. Therefore, some caution must be taken when using moving belts for flow modification or control. It would be preferable to measure local boundary layer flow under the actual operating conditions, rather than estimate it from expressions based on stationary-wall measurements.

References

[1] Katz, J., "Aerodynamics of Race Cars," *Annual Review of Fluid Mechanics*, Vol. 38, 2006, pp. 27–63.

[2] Berndtsson, A., Eckert, W. T., and Mercker, E., "The Effect of Groundplane Boundary Layer Control on Automotive Testing In a Wind Tunnel," Society of Automotive Engineers SAE 880248, 1988.

[3] Wiedemann, J., "Some Basic Investigations Into the Principles of Ground Simulation Techniques in Automotive Wind Tunnels," Society of Automotive Engineers SAE 890369, 1989.

[4] Modi, V. J., "Moving Surface Boundary-Layer Control: A Review," *Journal of Fluids and Structures*, Vol. 11, No. 6, 1997, pp. 627–663.

[5] Tokaty, G. A., *A History and Philosophy of Fluid Mechanics*, Dover Publications, Inc., New York, 1971.

[6] Bechert, D. W., Hage, W., and Brusek, M., "Drag Reduction with the Slip Wall," *AIAA Journal*, Vol. 34, No. 5, 1996, pp. 1072–1074.

[7] Choi, B., and Choi, H., "Drag Reduction with a Sliding Wall In Tow Over a Circular Cylinder," *AIAA Journal*, Vol. 38, No. 4, 2000, pp. 715–717.

[8] Uzkan, T., and Reynolds, W. C., "A Shear-Free Turbulent Boundary Layer," *Journal of Fluid Mechanics*, Vol. 28, Pt. 4, 1967, pp. 803–821.

[9] El Telbany, M. M. M., and Reynolds, A. J., "Velocity Distributions in Plane Turbulent Channel Flows," *Journal of Fluid Mechanics*, Vol. 100, Pt. 1, 1980, pp. 1–29.

[10] Aronson, D., Johansson, A. V., and Löfdahl, L., "Shear-Free Turbulence Near a Wall," *Journal of Fluid Mechanics*, Vol. 338, 1997, pp. 363–385.

[11] Bott, D. M., and Bradshaw, P., "Effect of High Free-Stream Turbulence on Boundary Layer Skin Friction and Heat Transfer," AIAA Paper 98-0531, 1998.

[12] Brungart, T. A., Lauchle, G. C., Deutsch, S., and Riggs, E. T., "Effect of a Moving Wall on a Fully Developed, Equilibrium Turbulent Boundary Layer," *Experiments in Fluids*, Vol. 30, No. 4, 2001, pp. 418–425.

[13] Nakabayashi, K., Kitoh, O., and Katoh, Y., "Similarity Laws of Velocity Profiles and Turbulence Characteristics of Couette-Poiseuille Turbulent Flows," *Journal of Fluid Mechanics*, Vol. 507, 2004, pp. 43–69.

[14] Tavoularis, S., *Measurement in Fluid Mechanics*, Cambridge Univ. Press, New York, 2005.

R. Lucht
Associate Editor